Fermi-edge singularity and the related emission from degenerate semiconductors: transition from a spontaneous to a stimulated process

Aika Tashiro,[1] Toshihiro Nakamura,[2] Yutaka Adachi,[3] Yoshiki Wada,[3] and Takashi Uchino[1]

[1]*Department of Chemistry, Kobe University, Nada, Kobe 657-8501, Japan*

[2] *Department of Electronic and Electronics, Hosei University, Koganei, Tokyo 184-8584, Japan*

[3]*Optical and Electronic Materials Unit, National Institute for Materials Science, Namiki 1-1, Tsukuba, 305-0044, Japan*

Abstract

We report on the observation of Fermi-edge singularity (FES) in the optical absorption and emission spectra of degenerate Ga-doped ZnO films from cryogenic to room temperature, as well as on the related stimulated emission under femtosecond laser pulse excitation. When the photo-generated electron-hole pair density n_{p} reaches a threshold, which is as low as $n_{\mathrm{p}}\sim10^{19}\mathrm{cm}^{-3}$ at room temperature, the emission from the Fermi edge shows a transition from a spontaneous to a stimulated regime, accompanied by a blue shift in the emission maximum. The observed low-threshold transition is consistent with the calculated gain spectra based on a quantum many-body theory.

In solid state physics, many-body effects, which are ultimately related to the correlation among electrons, are one of the most interesting, but also the most challenging, issues both in terms of experiments and theoretical treatments [1–4]. The primary difficulty is that a large number of electrons can interact through the infinite-range Coulomb force on an extremely short timescale (~10^{-12} s), enabling a coherent superposition of eigenstates not found in "free-electron" systems [3]. In photoexcited semiconductors, things will become more complicated because of the generation of photoexcited electrons and holes simultaneously. This leads to the formation of excitons or an electron-hole plasma (EHP) state depending on the density of the electron-hole pair [5]. In the Mott transition model, the exciton bound states cease to exist when the electron-hole pair density n_p exceeds the Mott density n_M [5]. In view of many-body physics, however, an exciton-like effect still survives even for $n_p > n_M$ due to the many-electron/one-hole interaction in the presence of the Fermi sea, which yields a "many-body" exciton, or a Mahan exciton [6]. Also, a divergence of optical oscillator strength occurs at the Fermi level of highly doped and highly excited semiconductors, giving rise to a so-called Fermi-edge singularity (FES) in optical absorption and emission spectra [7]. Thus, the observation of the FES and the Mahan exciton has been regarded as a hallmark of many-body effects and is still a topic of active research in the field of condensed matter

physics [8–20].

Although the FES has been reported to occur in various degenerate semiconductors, including highly-doped bulk [8–10,21–30] and modulation-doped quantum wells [31–35], stimulated light emission from the Fermi edge has hardly been observed. This appears to be strange because in degenerate semiconductors, their chemical potential is located well within the conduction (or valence) band already in equilibrium. According to the Bernard and Duraffourg (B-D) condition [36], the EHP gain at a temperature T is achieved when the electron-hole pair chemical potential μ with respect to the band gap ($\mu = \mu_e + \mu_h$) becomes greater than ~$2k_{\mathrm{B}}T$ [36,37], where μ_{e} (μ_{h}) is the quasi-chemical potential for electrons (holes) measured from the conduction(valence)-band edge and k_{B} is the Boltzmann constant. The B-D condition implies that the optical gain from an inverted EHP state could be in principle achieved for much lower values of n_{p} than that of the intrinsic one [38]. A possible reason for the difficulty in observing the Fermi-edge stimulated emission is that high doping induces lattice defects/strains and related non-radiative centers, which would potentially prevent the optical amplification. In the case of the modulation-doped quantum wells, the FES and the related emission tend to be removed when the density of photoexcited carriers is increased to a certain level due to the significant state broadening and damping of photoexcited holes [32].

Hence, the Fermi-edge stimulated emission is challenging to be realized, but it is worth investigating as it will provide a new insight into many-body effects and the related optical emission features in degenerate semiconductors.

In this letter, we overcome the problem using high-quality degenerate Ga-doped ZnO (GZO) films prepared by a pulsed laser deposition (PLD) method in highly optimized and controlled conditions. Previously, lasing characteristics of ZnO thin films, nanowires and nanoparticles were intensively investigated [39–45]. The threshold value of n_p for EHP lasing for nominally undoped ZnO nanosystems is reported to be as high as ~10^{19}–10^{20} cm^{-3} at room temperature [44,45], while the value of n_M is estimated to be ~2–6×10^{18} cm^{-3} at 300 K [46–48]. Although the FES was reported from highly-doped ZnO films with a carrier concentration higher than n_M [10], stimulated emission from the Fermi edge has not yet been reported. Here, we performed detailed optical absorption and photoluminescence (PL) measurements on the high-quality degenerate GZO samples from cryogenic to room temperature, along with calculations based on a quantum many-body theory. We then found that the present samples not only show the signature of the FES in the absorption and emission spectra, but they also demonstrate a transition from a spontaneous to a stimulated regime under relatively low excitation conditions even at room temperature.

A nominally undoped ZnO film and GZO thin films with donor concentration n_d ranging from $\sim 10^{16}$ to $\sim 10^{21}$ cm^{-3} were grown on an *a*-plane sapphire substrate [49,50] by PLD under the carefully optimized deposition condition (for details, see the Methods in the Supplemental Material [51]). All the ZnO and GZO thin films are c-axis oriented (Fig. S1(a) in the Supplemental Material [51]). For the GZO films with n_d from 8.7×10^{19} to 2.0×10^{20} cm^{-3}, the full width at half maximum (FWHM) values of X-ray rocking curves for the (0002) diffraction are comparable to that of the ZnO thin film (Fig. S1(b) in the Supplemental Material [51]). Note also that the carrier Hall mobility η is as high as 50–80 cm^{2}V^{-1}s^{-1} for the GZO films with n_d around 1.0×10^{20} cm^{-3}, whereas η decreases down to approximately 20 cm^{2}V^{-1}s^{-1} with a further increase in n_d up to $\sim 1 \times 10^{21}$ cm^{-3} (Fig. S2 in the Supplemental Material [51]). These results demonstrate that the high crystallinity is retained in our GZO samples as long as n_d is below 2×10^{20} cm^{-3}, which is still two orders higher than n_M in ZnO.

Figure 1(a) shows room-temperature optical absorption spectra for the ZnO film with the thickness D = 249 nm and $n_d = 2.7 \times 10^{16}$ cm^{-3} and three GZO films, which are termed GZO1 (D = 236 nm, $n_d = 8.7 \times 10^{19}$ cm^{-3}), GZO2 (D = 140 nm, $n_d = 1.3 \times 10^{20}$ cm^{-3}) and GZO3 (D = 320 nm, $n_d = 8.3 \times 10^{20}$ cm^{-3}). The ZnO film shows typical sharp exciton-related absorption peaks in the 3.3–3.4 eV energy range [39–43]. On the other

hand, such excitonic features are missing in the GZO samples; rather, the absorption spectra of GZO1 and GZO2 are characterized by a steep rise at the absorption edge and a slow fall at higher energies, which is a typical characteristic of the FES. Makino *et al.* [10] demonstrated that the absorption spectrum $A(E)$ showing the FES in degenerate ZnO can be described by the following power-law function [7] convoluted with a Gaussian distribution with a half-width Γ_{Gauss} [9],

$$A(E) = A_0(E) \int_{-\infty}^{+\infty} \left(\frac{\zeta_0}{E - E' - E_{\mathrm{th}}} \right)^{\alpha} \exp\left\{ -\left(\frac{E'}{\Gamma_{\mathrm{Gauss}}} \right)^2 \right\} dE' , \qquad (1)$$

where E is the energy of photon, α is the coupling parameter related to the strength of the attractive electron-hole interaction, ζ_0 is a cutoff energy, and E_{th} is the threshold energy where the optical absorption sets in and hence reflects the Fermi edge [7]. The term $A_0(E)$ contains the factor derived from the fundamental absorption [10,52,53] (for details, see the Supplemental Material [51]). We found that the observed room-temperature absorption spectra are well represented by Eq. (1), yielding the fitted values of $E_{\mathrm{th}} = 3.385$ and 3.435 eV for GZO1 and GZO2, respectively (a full list of the fitted parameters can be found in Table SI in the Supplemental Material [51]). However, the absorption spectrum of GZO3 is not fitted to Eq. (1) but can be well represented by the

following function taking into account only a Fermi-level filling factor [53,54]:

$$A(E) = A_0(E)\frac{1}{\left\{1+\exp\left(\frac{E_{abs}-E}{"kT"}\right)\right\}E^2}, \qquad (2)$$

where E_{abs} is the absorption edge shifted by the Burstein-Moss effect and $"kT"$ is a fitting parameter representing inhomogeneous (temperature) broadening. Hence, it is probable that the expected absorption anomaly is strongly smeared out in GZO3 due to the impurity effect.

If the room-temperature absorption spectra of GZO1 and GZO2 exhibit the FES, it could be possible to observe a similar singularity in the PL and PL excitation (PLE) spectra. Unfortunately, the PL emission intensities of GZO1 and GZO2 are too low to recognize the singularity at room temperature when measured by using a spectrofluorometer under Xe lamp excitation. Hence, we performed low-temperature emission and absorption measurements on GZO1 and GZO2 using a He-flow cryostat (see Fig. 1(b) and Fig. S3 in the Supplemental Material [51]). As for GZO3, however, we did not obtain analyzable PL signals even at temperatures below ~10 K. We found that the 6-K absorption spectra of GZO1 and GZO2 are well fitted to Eq. (1), as shown in Fig. 1(b), and the fitted values of E_{th} become higher than those at room temperature by ~0.05

eV. One also sees from Fig. 1(b) that the 6-K PL spectra of GZO1 and GZO2 show an asymmetric emission band peaking at 3.38 eV, whereas the corresponding PLE spectra exhibit a rapid increase in intensity at energies above E_{th}, resulting in a peak feature at ~3.5 eV. We consider that the observation of the ~3.5-eV peak in the PLE spectra provides additional evidence of the FES in these GZO samples. The PL band at 3.38 eV probably results from the emission from the Fermi edge to the acceptor levels due to Zn vacancy V_{Zn}, which is the main deep acceptor center in *n*-type ZnO [55]. This is because the observed Stokes-shift ΔE of the PL emission with respect to the PLE peak energy (ΔE~0.12 eV) is in good agreement with the ionization energy of the acceptor ($E_{\mathrm{A}}(V_{\mathrm{Zn}})$ = 0.12 eV) obtained from density functional calculations [55].

We next investigate the changes in the PL spectra of the GZO samples with excitation fluence (F_{ex}) under 100-fs pulse excitation at ~330 nm (~3.76 eV). The measurements were carried out at 6 K and room temperature. For the details of the experimental procedures, see the Methods in the Supplemental Material [51]. A series of 6-K PL spectra of GZO1 as well as the corresponding absorption spectrum are given in Fig. 2(a). For F_{ex} at 0.03 mJ/cm^2, the PL spectrum shows an asymmetric PL band peaking at ~3.38eV, in agreement with that obtained using a Xe lamp as an excitation source. When F_{ex} increases from 0.03 to 0.09 mJ/cm^2, the PL spectrum becomes narrow and symmetric, accompanied

by a blue shift of the peak energy by ~0.1 eV along with a significant (more than twenty times) increase in intensity. For higher excitation fluences, a substantial redshift of the peak energy and spectral broadening were observed, as often seen in the stimulated emission from an inverted EHP [5,43]. We also found that the PL decay curves become steeper for F_{ex} larger than 0.09 mJ/cm^2, as shown in Fig. 2(b). These changes in the spectral and decay features with F_{ex} allow us to confirm that a transition from the spontaneous emission to the EHP stimulated emission occurs at the threshold fluence of 0.09 mJ/cm^2, as schematically shown in the inset of Fig. 2(b). Considering that the emission peak energy at the threshold almost coincides with E_{th} (or the PLE peak energy), we can reasonably expect that the resulting stimulated emission is due to the recombination between the electrons at the Fermi edge and the holes in the valence band.

Further noteworthy is that a similar transition from a spontaneous to a stimulated emission regime is seen at room temperature [see Fig. 3(a) for GZO1 and Fig. S4 in the Supplemental Material [51] for GZO2]. Here, we should remind that nominally pure ZnO thin films, nanowires and nanopowders exhibit a room-temperature EHP stimulated emission as well [39−43]. In the case of the ZnO nanostructures, however, the stimulated emission occurs at a lower energy than the spontaneous emission [see, for example, Fig. 3(b)], which is different to the case of GZO1. Note also that the emission peak energy and

the half width of GZO1 are substantially higher and broader than those of ZnO although the threshold fluence of GZO1 (~0.2 mJ/cm^2) is an order lower than that of ZnO (~1 mJ/cm^2) [43–45]. We assume that these differences in the stimulated emission characteristics between GZO1 and ZnO originate from the inherently large chemical potential of degenerate semiconductors, as inferred in the Introduction section.

To confirm the above assumption, we calculated the room-temperature optical gain spectra $g(E)$ of GZO1, i.e., an *n*-doped ZnO with $n_d = 8.7\times 10^{19}$ cm^{-3}, on the basis of the quantum many-body theory developed by Versteegh and co-workers [46]. The details of the calculation procedures are given in [44–46], and a brief description on the calculation used here is shown in the Supplemental Material [51]. The theory was originally developed for the understanding of the optical spectra, charge-carrier screening, and carrier dynamics of ZnO at room temperature in the course of optical excitation, in which the net densities of electron *n* and hole *p* under photoexcitation are both equal to n_p. The theory is applicable to the photo-excited system with $n < 2.8 \times 10^{20}$ cm^{-3} [46], where charge-carrier screening is established fast with respect to the Fermi frequencies. Hence, we believe that this many-body theory is useful to understand the gain characteristics of degenerate systems at room temperature. In addition, μ_e and μ_h, both of which are required to calculate the screening length and the susceptibility in the

framework of the quantum many-body theory [44–46], were numerically determined within the parabolic band approximation (for details, see the Supplemental Material [51]).

Figure 4(a) shows how μ_e and μ_h of GZO1 (n_d = 8.7× 10^{19} cm^{-3}) change as n_p increase at a temperature of 300 K. For comparison, we also show in Fig. 4(a) the results on the ZnO sample with n_d of 2.7×10^{16} cm^{-3}. One sees from Fig. 4(a) that in GZO1, μ_e is already situated well above the bottom of the corresponding bands (μ_e~0.25 eV) even for $n_p < 1 \times 10^{17}$ cm^{-3}, whereas, in ZnO, μ_e dose not become positive until n_p reaches ~2×10^{18} cm^{-3}. On the other hand, the μ_h values in ZnO and GZO1 practically show the same n_p dependence, becoming positive for $n_p > \sim 1 \times 10^{19}$ cm^{-3}. These changes in μ_e and μ_h with n_p are reflected in the n_p dependence of $g(E)$, as shown in Fig. 4(b). As for GZO1 film with D = 236 nm, the photo-generated electron-hole pair density n_p at the room-temperature threshold fluence (F_{ex} = 0.23 mJ/cm^2) is estimated to be $n_p = 1.62 \times 10^{19}\text{cm}^{-3}$ from $n_p = F_{ex}/(\hbar\omega D)$ [44], where $\hbar\omega$ is the photon energy of the pump laser. It is clear from Fig. 4(b) that in GZO1, an optical gain appears at $n_p = 6.5 \times 10^{18}$ cm^{-3} and reaches ~1.4×10^4 cm^{-1} at 3.3 eV for $n_p = 1.62 \times 10^{19}\text{cm}^{-3}$. The resulting gain spectra are in reasonable agreement with the symmetric PL spectra observed for $F_{ex} \geq$ 0.23 mJ/cm^2 shown in Fig. 3(a). Although the present calculations yield the theoretical upper bound for $g(E)$, these calculations support the

occurrence of room-temperature stimulated emission from the GZO film in the present experimental condition. Note also that in ZnO, no gain occurs for $n_p = 1.62 \times 10^{19}\mathrm{cm}^{-3}$. These calculated results are consistent with the difference of EHP stimulated emission characteristics between GZO1 and ZnO shown in Fig. 3, i.e., a lowere threshold, a broader spectral width, and a higher peak energy of GZO1 than those of ZnO.

In summary, high-quality degenerate GZO films with n_d of ~1×10^{20} cm^{-3} show a signature of the FES in the absorption and PLE spectra, along with the EHP stimulated emission not only at cryogenic, but also at room temperature under the above-band-gap pulsed laser excitation conditions. At the threshold, the stimulated emission occurs at higher energies with respect to the spontaneous emission, yielding the peak energy corresponding to the Fermi-edge energy inferred from the absorption and PLE spectra. We then performed quantum many-body calculations to estimate the theoretical upper bound of the optical gain in GZO1 at room temperature. For the same value of n_p, GZO1 yields a much higher EHP gain than ZnO. Also, the calculated gain spectra of GZO1 are basically in agreement with the observed stimulated emission spectra. Hence, the present results demonstrate the transition of the Fermi-edge emission from a spontaneous to a stimulated regime, shedding new light on the absorption and emission processes in dense electron-hole systems in view of FES.

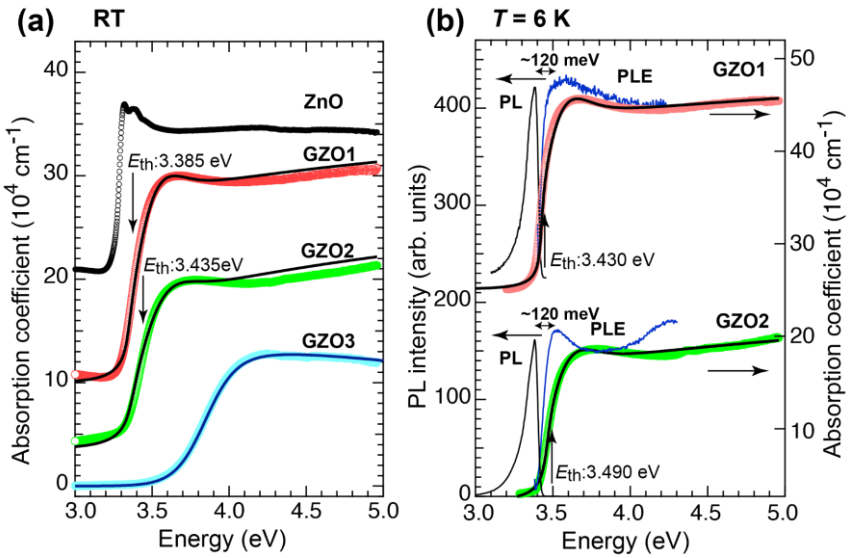

FIG. 1. (a) Room-temperature absorption spectra of ZnO film and three degenerate GZO films, termed GZO1, GZO2 and GZO3. (b) Low-temperature (6 K) absorption, PL and PLE spectra of GZO1 and GZO2. Respective spectra are shifted vertically for clarity. The solid lines for GZO1 and GZO2 are the fit to Eq. (1), showing the fitted values of E_{th}. The solid line for GZO3 is the fit to Eq. (2).

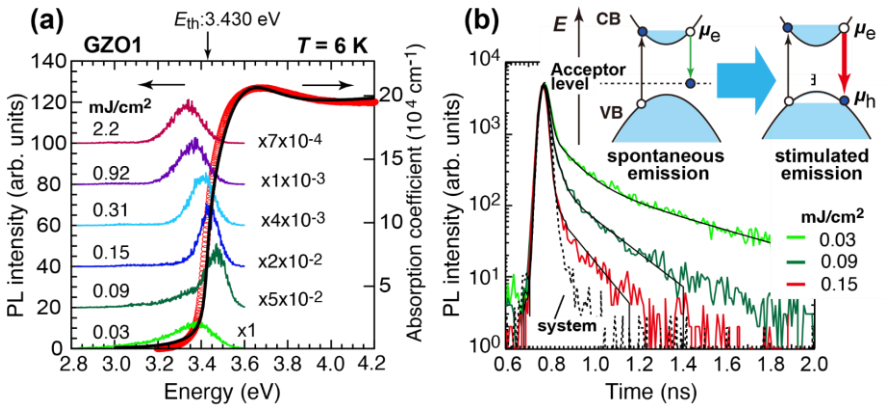

FIG. 2. (a) (Left scale) Excitation fluence F_{ex} dependence of the low-temperature (6 K) PL spectra of GZO1 under 100-fs pulse excitation at 332 nm. PL spectra are shifted and scaled by the factor given in the right side of the respective spectra. (Right scale) The low-temperature (6 K) absorption coefficient spectrum of GZO1 (red open circles) and the fit to Eq. (1) (solid line), showing the fitted value of E_{th} on the upper horizontal axis. (b) The decay profile of the emission obtained under different excitation fluences indicated. Each solid line represents the fitted convolution curve between the laser pulse and a double exponential function. The fitted decay times (τ_1 and τ_2) under excitation fluences of 0.03, 0.09 and 0.15 mJ/cm^2 are 0.10 and 0.50 ns, 0.04 and 0.20 ns, and 0.01 and 0.13 ns, respectively. The inset in (b) schematically shows a transition of the emission process from a spontaneous to a stimulated regime.

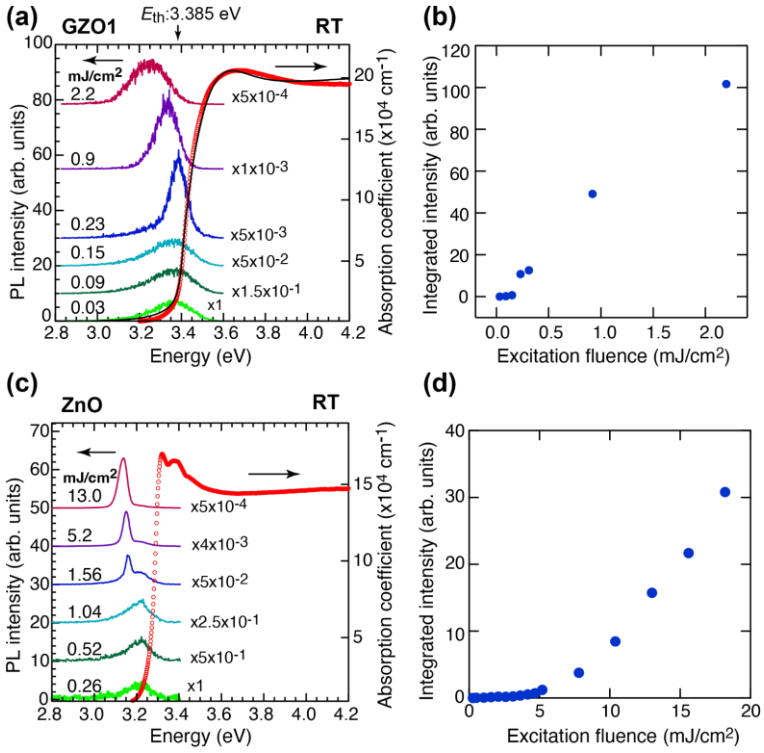

FIG. 3. (a, c) Excitation fluence F_{ex} dependence of the room-temperature PL spectra of (a) GZO1 under 100-fs pulse excitation at 332 nm and (c) ZnO under 10-ns pulse excitation at 355 nm. PL spectra are shifted and scaled by the factor given in the right-hand side of the respective spectra. The corresponding room-temperature absorption coefficient spectra (red open circles) are given in the right scale. The black solid line in (a) is the fit to Eq. (1), showing the fitted value of E_{th} on the upper horizontal axis. (b,d) The energy-integrated PL intensity of (b) GZO1 and (d) ZnO as a function of F_{ex}.

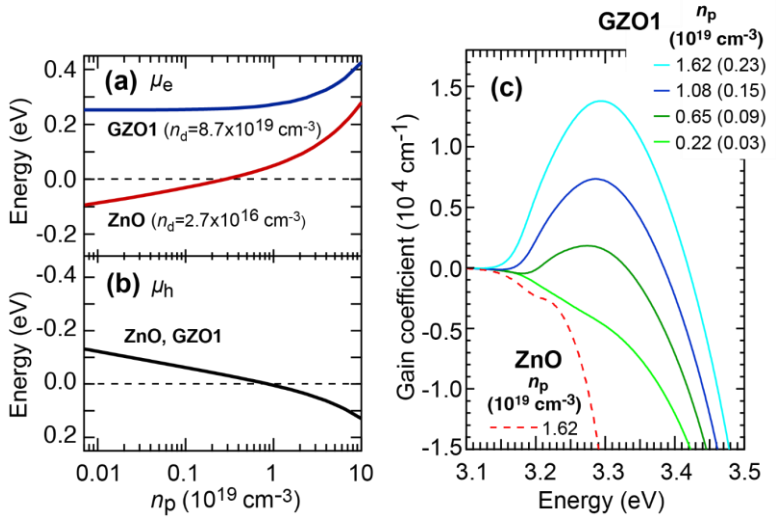

FIG. 4. Changes in (a) μ_e and (b) μ_h as a function of photo-generated electron hole density n_p calculated at 300 K for ZnO and GZO1. The dashed lines in (a) and (b) indicate the reference energy level of the conduction band (conduction band minimum) and that of the valence band (valence band maximum), respectively. (c) Theoretical gain spectra of GZO1 calculated at 300 K for different values of n_p. The values in parenthesis represent the corresponding excitation fluences (units in mJ/cm^2) under the present 100-fs excitation condition. The 300-K gain spectrum of ZnO for $n_p = 1.62 \times 10^{19}$ cm^{-3} is also shown for comparison.

References

[1] G. D. Mahan, *Many-particle Physics,* 3rd ed. (Plenum, New York, 2000).

[2] P. Coleman, *Introduction to Many-Body Physics* (Cambridge University Press, Cambridge, 2016).

[3] D. S. Chemla and J. Shah, Many-body and correlation effects in semiconductors, Nature **411**, 549 (2001).

[4] M. Kira and S.W. Koch, Many-body correlations and excitonic effects in semiconductor spectroscopy, Prog. Quantum Electron. **30**, 155 (2006).

[5] C. F. Klingshirn, *Semiconductor Optics*, 2nd ed. (Springer, Berlin, 2005) pp.521-552.

[6] G. D. Mahan, Excitons in degenerate semiconductors, Phys. Rev. **153**, 882 (1967).

[7] G. D. Mahan, Excitons in metals: infinite hole mass, Phys. Rev. **163**, 612 (1967).

[8] M. Feneberg, S. Osterburg, K. Lange, C. Lidig, B. Garke, R. Goldhahn, E. Richter, C. Netzel, M. D. Neumann, N. Esser, S. Fritze, H. Witte, J. Bläsing, A. Dadgar, and A. Krost, Band gap renormalization and Burstein-Moss effect in silicon- and germanium-doped wurtzite GaN up to 10^{20} cm^{-3}, Phys. Rev. B **90**, 075203 (2014).

[9] F. Fuchs, K. Kheng, P. Koidl, and K. Schwarz, Fermi-edge singularity in degenerate n-type bulk InAs, Phys. Rev. B **48**, 7884 (1993).

[10] T. Makino, K. Tamura, C. H. Chia, Y. Segawa, M. Kawasaki, A. Ohtomo, and H. Koinuma, Optical properties of ZnO:Al epilayers: Observation of room-temperature many-body absorption-edge singularity, Phys. Rev. B **65**, 121201(R) (2002).

[11] P. Karnatak, S. Goswami, V. Kochat, A. N. Pal, and A. Ghosh, Fermi-edge

transmission resonance in graphene driven by a single coulomb impurity, Phys. Rev. Lett. **113**, 026601 (2014).

[12] N. A. J. M. Kleemans, J. van Bree, A. O. Govorov, J. G. Keizer, G. J. Hamhuis, R. Nötzel, A. Yu. Silov, and P. M. Koenraad, Many-body exciton states in self-assembled quantum dots coupled to a Fermi sea, Nat. Phys. **6**, 534 (2010).

[13] P. Plochocka-Polack, J. G. Groshaus, M. Rappaport, V. Umansky, Y. Gallais, A. Pinczuk, and I. Bar-Joseph, Fermi-edge singularity of spin-polarized electrons, Phys. Rev. Lett. **98**, 186810 (2007).

[14] J.-H. Kim, G. T. Noe II, S. A. McGill, Y. Wang, A. K. Wójcik, A. A. Belyanin, and J. Kono, Fermi-edge superfluorescence from a quantum-degenerate electron-hole gas, Sci. Rep. **3**, 3283 (2013).

[15] T. Palmieri, E. Baldini, A. Steinhoff, A. Akrap, M. Kollár, E. Horváth, L. Forró, f. Jahnke, M. Chergui, Mahan excitons in room-temperature methylammonium lead bromide perovskites. Nat. Commun. **11**, 850 (2020).

[16] S. Gao, Y. Liang, C. D. Spataru, and L. Yang, Dynamical excitonic effects in doped two-dimensional semiconductors, Nano Lett. **16**, 9, 5568 (2016).

[17] D. Pimenov and M. Goldstein, Spectra of heavy polarons and molecules coupled to a Fermi sea, Phys. Rev. B **98**, 220302(R) (2018).

[18] D. J. Choksy, E. A. Szwed, L. V. Butov, K. W. Baldwin, and L. N. Pfeiffer, Fermi edge singularity in neutral electron–hole system, Nat. Phys. **19**, 1275 (2023).

[19] Y.-W. Chang and D. R. Reichman, Many-body theory of optical absorption in doped two-dimensional semiconductors, Phys. Rev. B **99**, 125421 (2019).

[20] C. Jackson and B. Braunecker, Spatiotemporal spread of Fermi-edge singularity as time-delayed interaction and impact on time-dependent RKKY-type coupling,

Phys. Rev. Research **4**, 013119 (2022).

[21] H. van Cong, S. Charar, and S. Brunet, Band-gap narrowing due to many body effects in *n*-Type degenerate GaAs Crystals, Phys. Status Solidi B **147**, 253 (1988).

[22] D. M. Szmyd; P. Porro; A. Majerfeld; S. Lagomarsino, Heavily doped GaAs:Se. I. Photoluminescence determination of the electron effective mass, J. Appl. Phys. **68**, 2367 (1990).

[23] H. D. Chen; M. S. Feng; P. A. Chen; K. C. Lin; C. C. Wu, Low-temperature luminescent properties of degenerate p-type GaAs grown by low-pressure metalorganic chemical vapor deposition, J. Appl. Phys. **75**, 2210 (1994).

[24] M. A. Reshchikov and H. Morkoç, Luminescence properties of defects in GaN, J. Appl. Phys. **97**, 061301 (2005).

[25] K. Ueno, T. Fudetani, Y. Arakawa, A. Kobayashi, J. Ohta, and H. Fujioka, Electron transport properties of degenerate n-type GaN prepared by pulsed sputtering, APL Mater. **5**, 126102 (2017).

[26] S. Shokhovets, K. Köhler, O. Ambacher, and G. Gobsch, Observation of Fermi-edge excitons and exciton-phonon complexes in the optical response of heavily doped *n*-type wurtzite GaN, Phys. Rev. B **79**, 045201 (2009).

[27] H. P. He, H. P. Tang, Z. Z. Ye, L. P. Zhu, B. H. Zhao, L. Wang, X. H. Li, Temperature-dependent photoluminescence of quasi aligned Al-doped ZnO nanorods, Appl. Phys. Lett. **90**, 023104 (2007).

[28] Z. Yang, D. C. Look, J. L. Liu, Ga-related photoluminescence lines in Ga-doped ZnO grown by plasma-assisted molecular-beam epitaxy, Appl. Phys. Lett. **94**, 072101 (2009).

[29] H. C. Park, D. Byun, B. Angadi, D. Hee Park, W. K. Choi, J. W. Choi, Y. S. Jung, Photoluminescence of Ga-doped ZnO film grown on c-Al_2O_3 (0001) by plasma-assisted molecular beam epitaxy, J. Appl. Phys. **102**, 073114 (2007).

[30] T. Makino, Y. Segawa, S. Yoshida, A. Tsukazaki, A. Ohtomo, M. Kawasaki, Gallium concentration dependence of room-temperature near-band-edge luminescence in *n*-type ZnO:Ga, Appl. Phys. Lett. **85**, 759 (2004).

[31] M. S. Skolnick, J. M. Rorison, K. J. Nash, D. J. Mowbray, P. R. Tapster, S. J. Bass, and A. D. Pitt, Observation of a many-body edge singularity in quantum-well luminescence spectra, Phys. Rev. Lett. **58**, 2130 (1987).

[32] H. Kalt, K. Leo, R. Cingolani, and K. Ploog, Fermi-edge singularity in heavily doped GaAs multiple quantum wells, Phys. Rev. B **40**, 12017(R) (1989).

[33] W. Chen, M. Fritze, W. Walecki, A. V. Nurmikko, D. Ackley, J. M. Hong, and L. L. Chang, Excitonic enhancement of the Fermi-edge singularity in a dense two-dimensional electron gas, Phys. Rev. B **45**, 8464 (1992).

[34] V. Huard, R. T. Cox, K. Saminadayar, A. Arnoult, and S. Tatarenko, Bound states in optical absorption of semiconductor quantum wells containing a two-dimensional electron gas, Phys. Rev. Lett. **84**, 187 (2000).

[35] H. Kissel, U. Zeimer, A. Maaßdorf, M. Weyers, R. Heitz, D. Bimberg, Yu. I. Mazur, G. G. Tarasov, Vas. P. Kunets, U. Müller, Z. Ya. Zhuchenko, and W. T. Masselink, Behavior of the Fermi-edge singularity in the photoluminescence spectra of a high-density two-dimensional electron gas, Phys. Rev. B **65**, 235320 (2002).

[36] M. G. A. Bernard and G. Duraffourg, Laser conditions in semiconductors, Phys. Status Solidi B **1**, 699 (1961).

[37] J. I. Pankove, *Optical Processes in Semiconductors* (Dover, New York, 1971) p. 216.

[38] L. Carroll, P. Friedli, S. Neuenschwander, H. Sigg, S. Cecchi, F. Isa, D. Chrastina, G. Isella, Y. Fedoryshyn, and J. Faist, Direct-gap gain and optical absorption in germanium correlated to the density of photoexcited carriers, doping, and strain, Phys. Rev. Lett. **109**, 057402 (2012).

[39] C. Klingshirn, ZnO: From basics towards application, Phys. Stat. Sol. B **244**, 3027 (2007).

[40] *Zinc Oxide: From Fundamental Properties Towards Novel Applications, Springer Series in Materials Science*, edited by C. F. Klingshirn, B. K. Meyer, A. Waag, A. Hoffmann, and J. Geurts (Springer, Belin, 2010).

[41] *Zinc Oxide: Fundamentals, Materials and Device Technology*, edited by H. Morkoç and Ü. Özgür (Wiley-VCH, Weinheim, 2009).

[42] *Zinc Oxide Materials for Electronic and Optoelectronic Device Applications*, edited by C. Litton, D. C. Reynolds and T. C. Collins (Wiley, Chichester, 2011).

[43] A. Tashiro, Y. Adachi, and T. Uchino, Excitonic processes and lasing in ZnO thin films and micro/nanostructures, J. Appl. Phys. **133**, 221101 (2023).

[44] M. A. M. Versteegh, D. Vanmaekelbergh, and J. I. Dijkhuis, Room-temperature laser emission of ZnO nanowires explained by many-body theory, Phys. Rev. Lett. **108**, 157402 (2012).

[45] T. Nakamura, K. Firdaus, and S. Adachi, Electron-hole plasma lasing in a ZnO random laser, Phys. Rev. B **86**, 205103 (2012).

[46] M. A. M. Versteegh, T. Kuis, H. T. C. Stoof, and J. I. Dijkhuis, Ultrafast screening and carrier dynamics in ZnO: Theory and experiment, Phys. Rev. B **84**, 035207

(2011).

[47] E. Hendry, M. Koeberg, and M. Bonn, Exciton and electron-hole plasma formation dynamics in ZnO, Phys. Rev. B **76**, 045214 (2007).

[48] A. Schleife, C. Rödl, F. Fuchs, K. Hannewald, and F. Bechstedt, Optical absorption in degenerately doped semiconductors: Mott transition or Mahan excitons? Phys. Rev. Lett. **107**, 236405 (2011).

[49] P. Fons, K. Iwata, A. Yamada, K. Matsubara, S. Niki, K. Nakahara, T. Tanabe, H. Takasu, Uniaxial locked epitaxy of ZnO on the a face of sapphire, Appl. Phys. Lett. **77**, 1801 (2000).

[50] Y. Xie, M. Madel, T. Zoberbier, A. Reiser, W. Jie, . Neuschl, J. Biskupek, U. Kaiser, M. Feneberg, and K. Thonke, Enforced c-axis growth of ZnO epitaxial chemical vapor deposition films on *a*-plane sapphire, Appl. Phys. Lett. **100**, 182101 (2012).

[51] See Supplemental Material at http://link.aps.org/ supplemental/ for further details of the sample preparation and measurements and a description of many-body theory calculations, along with additional experimental data.

[52] A. R. Goñi, A. Cantarero, K. Syassen, and M. Cardona, Effect of pressure on the low-temperature exciton absorption in GaAs, Phys. Rev. B **41**, 10111 (1990).

[53] M. Muñoz, F. H. Pollak, M. Kahn, D. Ritter, L. Kronik, and G. M. Cohen, Burstein-Moss shift of n-doped In0.53Ga0.47As/InP, Phys. Rev. B **63**, 233302 (2001).

[54] J. D. Ye, S. L. Gu, S. M. Zhu, S. M. Liu, Y. D. Zheng, R. Zhang, Y. Shi, Fermi-level band filling and band-gap renormalization in Ga-doped ZnO, Appl. Phys. Lett. **86**, 192111 (2005).

[55] A. Janotti and C. G. Van de Walle, Native point defects in ZnO, Phys. Rev. B **76**, 165202 (2007).